Chapter 5

Phase separation kinetics of binary mixture in the influence of bond disorder

5.1 Introduction

When a binary (AB) mixture is uniformly mixed at temperatures above the critical point ($T > T_c$, where $T_c = 2.269J/k_B$), it appears homogeneous. However, upon cooling below the critical temperature ($T < T_c$), the mixture becomes thermodynamically unstable due to minor irregularities within the system. At this point, the mixture undergoes phase separation via either spinodal decomposition (SD) [6,8–10,12] or nucleation and growth (NG) [6,8,9,12], resulting in distinct regions enriched in one of the components.

The study of phase separation kinetics has been a highly active and robust area of research [99,217–222] for many years. Researchers use experimental [223–225], analytical [9,226–229], and simulation approaches [19,217,230–232] to explore how binary mixtures evolve. To understand the morphologies of the phase seperating system, researchers often examine two important physical attributes: (i) the two-point equal-time correlation function $C(\vec{r},t)$, where $\vec{r} = \vec{r}_1 - \vec{r}_2$, and its Fourier transform, the structure factor $S(\vec{k},t)$, with $\vec{k}$ representing the wave vector [9,10]; (ii) the domain growth law, which describes how the size of characteristic

domains increases over time. This growth law is affected by various system properties, such as conservation laws, hydrodynamic velocity fields [233,234], and the presence of quenched or annealed disorder [217,235–237].

If a system is purely isotropic, then at later times, the domain growth law generally shows power-law behavior: $l(t) \sim t^{\phi}$, where ϕ represents the growth exponent [9,10]. The value of ϕ is determined by the mechanism that driving the coarsening. For the diffusion-driven segregation of conserved AB mixture, the rate of domain evolution yields $\dot{l}(t) \sim |\vec{\nabla}\mu| \sim \sigma/t^2$ provides $l(t) \sim t^{1/3}$, known as the Lifshitz-Slyozov (LS) growth law with a growth exponent of $\phi = 1/3$ [9,10,238]. Here, the interface velocity is represented by $\dot{l}(t)$, the chemical potential by μ, and the interfacial tension between the phases by σ. It is worth noting that depending on the dimensionality and other system parameters, multiple growth regimes can emerge due to hydrodynamic forces in the system [233,234,239–241].

Due to the presence of impurities, it is challenging to find a pure and isotropic experimental system (either annealed or quenched). Consequently, various significant studies have been conducted on the $2d$ Ising model with quenched disorder [226,230,231,235,236,242,243], both analytically and numerically. The quenched disorder is considered an immobile impurity in the system and is incorporated in two ways in a pure Ising system: (i) through the random-field Ising model (RFIM) [244–247] and (ii) through the random-bond Ising model (RBIM) [235,236,243] using *nn* spin-exchange kinetics. The disordered sites have the capability to trap domain boundaries, which in turn slows down domain expansion. Huse and Henley (HH) [248] conduct a critical analysis of RBIM for the non-conserved system.

According to their argument, the energy barrier (E_b) depends on the domain size (l) as $E_b(l) \sim \varepsilon l^{\psi}$, where ε indicates the disorder/impurity strength and ψ is the barrier exponent. The barrier exponent, $\psi = \chi/(2-\zeta)$, where the roughening (ζ) and pinning (χ) exponents are related as $\chi = 2\zeta + d - 3$ and d represents the system dimensionality. The characteristic length scale behaves logarithmically as $l(t) \sim (\ln t)^{\phi}$, and computational [19,226,230–232,237,242,

243]. Many experimental studies [223–225] have been conducted to evaluate the HH concept. However, an alternative with a power-law growth and a variable exponent has been proposed.

Paul, Puri, and Rieger (PPR) conducted a thorough reexamination of the RBIM using MC simulations of kinetic Ising models. These models featured conserved spin-exchange kinetics [235,236] and non-conserved spin-flip kinetics. Rather than using a power law, PPR suggested that the energy barrier for trapping domain boundaries would have a logarithmic dependence on the domain size: $E_b(l) \sim \varepsilon \ln(1+l)$ [235,236]. The growth exponent $\theta(\varepsilon, T) = 1/(3+\varepsilon T^{-1})$ depends on the quench depth (T) and impurities (ε) in the system. PPR demonstrated a power-law dependence: $l(t) \sim A(\varepsilon, T)t^{\theta(\varepsilon,T)}$ on the average domain size; these findings were further confirmed experimentally [223,225]. The system evolves like a pure system because, overall, the energy barrier becomes insignificant due to the small average domain size. On the other hand, a higher energy barrier at later times causes disorder traps to become effective beyond a certain length scale. As a result, thermal activation (characterized by $k_B T$) across the relevant energy barrier ($E_b(l)$) [248] leads to domain coarsening. In contrast to the pure case where thermal fluctuations are insignificant, thermal fluctuations drive the expansion of the domain at later times [234,235].

HH and PPR have introduced quenched disorder by uniformly varying the spin coupling strength between zero and one for all the nearest neighbor (*nn*) sites [235,236,248]. A few recent studies [217,222] have shown how the quenched disorder affects the $2d$ Ising system when bond disorder (BD) is introduced in two ways: (i) randomly and (ii) regularly [217]. The studies examined the evolution kinetics only at a modest quench temperature $(T = 1.0)$ and up to an intermediate duration ($t = 1.6 \times 10^6$ MCS). For both the conserved and nonconserved $2d$ Ising systems, it was found that the length scale strongly depended on the bond disorder. The dynamic scaling functions for the conserved system showed a significant deviation from the master function when random bond disorder was introduced. However, a similar scaling function behavior was observed with higher regular bond disorder. It was only at the higher

regular bond disorder that the crossing of the length scale from $\phi = 1/3$ to $1/2$ due to random diffusion at the domain interfaces was observed. Nevertheless, at the lower bond disorder, the length scales mostly remained in the LS growth regimes, with a slight crossover to a more significant growth exponent observed until the simulation duration at $t = 1.6 \times 10^6$ MCS at $T = 1.0$ [217,222].

In our current research, we are studying the effects of shallow $(T = 1.5)$ and deep $(T = 0.5)$ quenches on the segregation kinetics of different fractions of BD that are regularly introduced [217,222]. To better understand how shallow or deep quench depth affects the ultimate equilibrium morphology at varying fractions of BD, we allowed the system to evolve for a longer period ($t = 4.0 \times 10^6 4$ MCS) than in previous studies [217,222]. Additionally, we decided to revisit the moderate quench situation $(T = 1.0)$ since it was not explored at the asymptotic time limit ($t = 4.0 \times 10^6$ MCS), especially at a smaller proportion of BD. Generally, we aim to understand how both deep and shallow quenches impact dynamic universality and domain growth in systems with BD. Theoretical calculations for this are usually much more complex.

We organize this work as follows. First, in Sec. 5.2, we briefly explain the numerical methodology used to simulate the system. Then, Sec. 5.3 presents the results and discussions for different temperatures and the fraction of BD. Finally, in Sec. 5.4, we conclude this work with a summary of our results.

5.2 Simulation model and implementation

5.2.1 Basic step with disordered site

MC simulation method is utilized to study the effect of BD in the $2d$ Ising system. The initial detail of MC simulation is given in Section 1.8.

In our simulation, we have chosen a square lattice with dimensions $N = L_x \times L_y$, where $L_x = L_y = 512$, and have applied periodic boundary conditions in both directions. The degree of disorder is represented by the exchange coupling parameter J_{ij}, which is defined as $1 - \varepsilon$. Here, ε quantifies the degree of disorder. For simplicity, we consider two extreme cases: (i) $\varepsilon = 0$, which represents pure *nn* sites, and (ii) $\varepsilon = 1$, which links to a disordered site in a *nn* spin pair (system's impurity). When $J_{ij} = 1$, it means we are connecting two pure neighboring sites, and when $J_{ij} = 0$, it signifies that at least one of the two neighboring sites is impure (disordered). It is important to note that $J_{ij} = 0$ indicates maximum disorder, where spins can take random up-down configurations. In other words, the related sites behave as if they are at a high temperature $T \gg T_c$, allowing all the proposed spin exchanges.

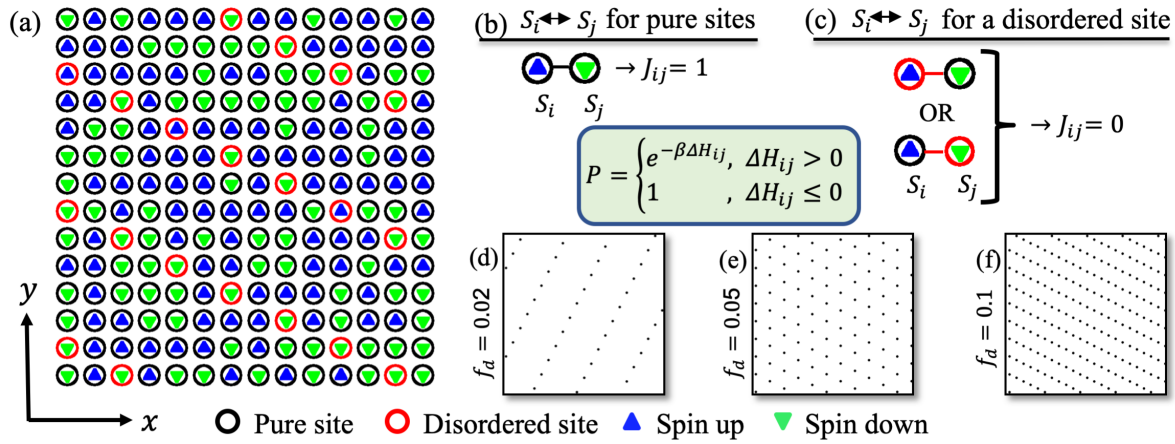

Fig. 5.1: The $2d$ Ising model on a square lattice is depicted in the following images. In (a), black circles represent pure sites, while red circles represent disordered sites with up (blue triangles) and down (green triangles) spins randomly assigned. (b) and (c) illustrate the standard Kawasaki spin-exchange kinetics probability and the exchange interaction (J_{ij}) between neighboring spins: (b) when two nearest-neighbor (*nn*) spins are at pure sites, and (c) when at least one *nn* spin is at a disordered site. Moreover, (d-f) show sections of disordered sites on a $2d$ square lattice of size $N = L^2$, where $L = 512$, for disorder fractions (f_d) of 0.02, 0.05, and 0.1, respectively. This figure provides a comprehensive visual representation of the Ising model with disordered sites.

The schematic diagrams in Figs. 5.1(a)-(c) illustrate the relevant configuration of up and down spins, tagged on pure and disordered sites. It is important to note that PPR's RBIM study involved a uniform distribution of J_{ij} values within the range $(0, 1)$. Thus, our study

is a limiting case of PPR's study regarding the value of exchange coupling strength. To introduce the disorder, we select a fraction of sites in a regular manner, as displayed in Fig. 5.1(a) schematically with red circles. When traversing the lattice indexes from 1 to L_x in the x-direction and 1 to L_y in the y-direction, every m^{th} site is designated as a disordered site. Consequently, the total number of disordered sites in a system is $N_d = f_d N$, where $f_d = 1/m$ represents the fraction of disordered sites. In Figs. 5.1(d)-(e), a section of disordered sites with f_d values of $0.02, 0.05$, and 0.1, respectively, is displayed on a $2d$ square lattice of size $N = L^2$, where $L = 512$.

The Ising model by itself does not exhibit inherent dynamics. To introduce stochastic dynamics, the system is put in contact with a heat bath. The resulting dynamical model is then called the kinetic Ising model [10]. In order to describe phase separation in a binary (AB) mixture, we can use the Kawasaki spin-exchange (conserved) kinetics. In this conserved kinetics, we randomly select two *nn* sites with opposite spins ($S_i \longleftrightarrow S_j$) to exchange. The energy change for the spin-exchange to take place is provided by [96]:

$$\Delta H_{ij} = 2S_i \left[\sum_{i' \neq j}^{q} J_{ii'} S_i - \sum_{j' \neq i}^{q} J_{jj'} S_{j'} \right]$$

Here, q represents the coordination number of a site. the symbols i' and j' denote the nearest neighbor sites of i and j sites, respectively. The spin-exchange is then either accepted or rejected based on the standard Metropolis acceptance probability:

$$P = \begin{cases} e^{-\beta \Delta H_{ij}}, & \Delta H_{ij} > 0, \\ 1, & \Delta H_{ij} \leq 0, \end{cases}$$

where $\beta = 1/k_B T$. The unit of time for all the following analyses is one Monte Carlo step (MCS), which consists of $N = L_x \times L_y$ spin-exchange attempts by using spin-exchange probability equation.

The initial configuration of a critical AB mixture, as shown in Fig. 5.1(a), corresponds to a uniform state of the system at a high temperature ($T \gg T_c$), with a random distribution of A ($S_i = +1$) and B ($S_i = -1$) atoms in a 1 : 1 ratio. This suggests that at high temperatures, there is no interaction ($J_{ij} = 0$) between the spins. As a result, the opposite spin pair *nn* has an exchange probability of $P \to 1$. To start the evolution, the uniform system is then rapidly quenched below T_c. In the long-time limit, which is mostly unexplored for the Ising systems, we study the influence of BD on the evolution morphologies, growth kinetics, dynamic universality, and sensitivity to shallow and deep quenches at $T = 0.5, 1.0$, and 1.5. In short, we present the results for various quench depths at three different fractions of disorder, $f_d = 0.02$, 0.05, and 0.1 (see the graphical illustration in Fig. 5.1(d)-(f)) and compare them with the pure case ($f_d = 0.0$).

5.2.2 Correlation function and structure factor

To investigate the evolution of morphology and length scale, we calculate the two-point equal-time correlation function [9,10] to measure the overlap of spin configurations at a distance $\vec{r}$:

$$C(\vec{r},t) = \frac{1}{N}\sum_i [\langle S_i(t) S_{i+\vec{r}(t)} \rangle - \langle S_i(t) \rangle \langle S_{i+\vec{r}(t)} \rangle]$$

The angular brackets represent the statistical averaging of data. The structure factor, an experimentally more relevant physical parameter to study the domain morphology, is the Fourier transform of $C(\vec{r},t)$ [9,10]:

$$S(\vec{k},t) = \sum_{\vec{r}} e^{i\vec{k}\vec{r}} C(\vec{r},t)$$

where $\vec{k}$ is the vector of the scattering wave. When the evolved morphologies are isotropic, the correlation function and the structure factor statistics can be improved by spherical averaging.

The corresponding quantities are denoted as $C(r,t)$ and $S(k,t)$, respectively, where r is the separation between two spatial points and k is the magnitude of wave-vector. The correlation function and the structure factor data are spherically average over ten independent runs unless stated otherwise. For the anisotropic morphologies in the system, we compute the component of the structure factor in different directions.

5.2.3 Scaling functions and length scale

The phenomenon of domain coarsening is a well-established scaling behavior that is characterized by a unique length scale, $l(t)$. The correlation function and the structure factor follow specific dynamical scaling forms:

$$C(r,t) \sim g[r/l(t)],$$

$$S(k,t) \sim l(t)^d f[kl(t)]$$

where, $g(x)$ and $f(p)$ are the scaling functions. The characteristic length scale, $l(t)$, is estimated from the correlation function as the distance over which it decays to zero or a fraction of its maximum value, $C(0,t) = 1$ [99]. We observe that the decay of $C(r,t)$ to 0.1 provides a good measure of $l(t)$. Some other definitions of length scale include (i) the inverse of the first moment of the structure factor [99] and (ii) the first moment of the normalized domain-size distribution [249,250]. These definitions differ only by constant multiplicative factors in the scaling regime [99,249,250]. We determined the asymptotic growth exponent by computing an effective growth exponent as follows [248,251,252]:

$$\phi_{eff} = \log_\alpha \left[\frac{l(\alpha t)}{l(t)}\right]$$

where we set the log-base $\alpha = 2$.

5.3 Simulation results and discussion

After quenching the system from a high-temperature homogeneous phase to a temperature below the critical temperat1ure ($T < T_c$), we observed the evolution of the system at different MCS. In our analysis, we focused on (i) how different fractions of disorder ($f_d = 0.02, 0.05,$ and 0.1) affected the coarsening patterns at shallow and deep quench depths ($T < T_c$), and (ii) how f_d and quench depths influenced the typical growth laws and scaling behavior of the system at late times.

5.3.1 Pure binary mixture: $f_d = 0.0$

At the outset of our simulation and to keep the rest of the results in proper context, we first illustrate the well-known kinetics for pure case ($\varepsilon_{ij} = 0, f_d = 0.0$) at three quench temperatures in Fig. 5.2. At $t = 4 \times 10^6$ MCS, the evolution morphologies for (a) $T = 0.5$, (b) $T = 1.0$, and (c) $T = 1.5$ are depicted in Fig. 5.2. Following the quench, the system demonstrates a characteristic interconnected, bi-continuous morphology as it grows and develops new domains via SD. The presence of A-rich morphology is denoted in maroon and B-rich is unmarked. At the early stage (transient regime) of demixing, even at $t \approx O(10^6)$ MCS, is caused by minimal thermal fluctuations k_BT at $T = 0.5$ (deep quench) [9,10,12]. At moderate to shallow quenches, the system displays typical domain patterns at temperatures of $T = 1.0$ and $T = 1.5$, respectively, over the same time period. The morphology at $T = 1.5$ (Fig. 5.2(c)) appears slightly more fuzzier due to higher thermal noise than the other two lower temperatures shown in Figs. 5.2(a)-(b). The spatial intensity fluctuation of the structural factor, $S(k_x, k_y)$, is depicted in the insets in Figs. 5.2(a)-(c), demonstrating isotropic domain evolution. The color bars on the right indicate the range of values for scattering intensity for each temperature, suggesting that the domain evolution is at an early stage for $T = 0.5$ and proceeds at a faster pace for $T = 1.5$.

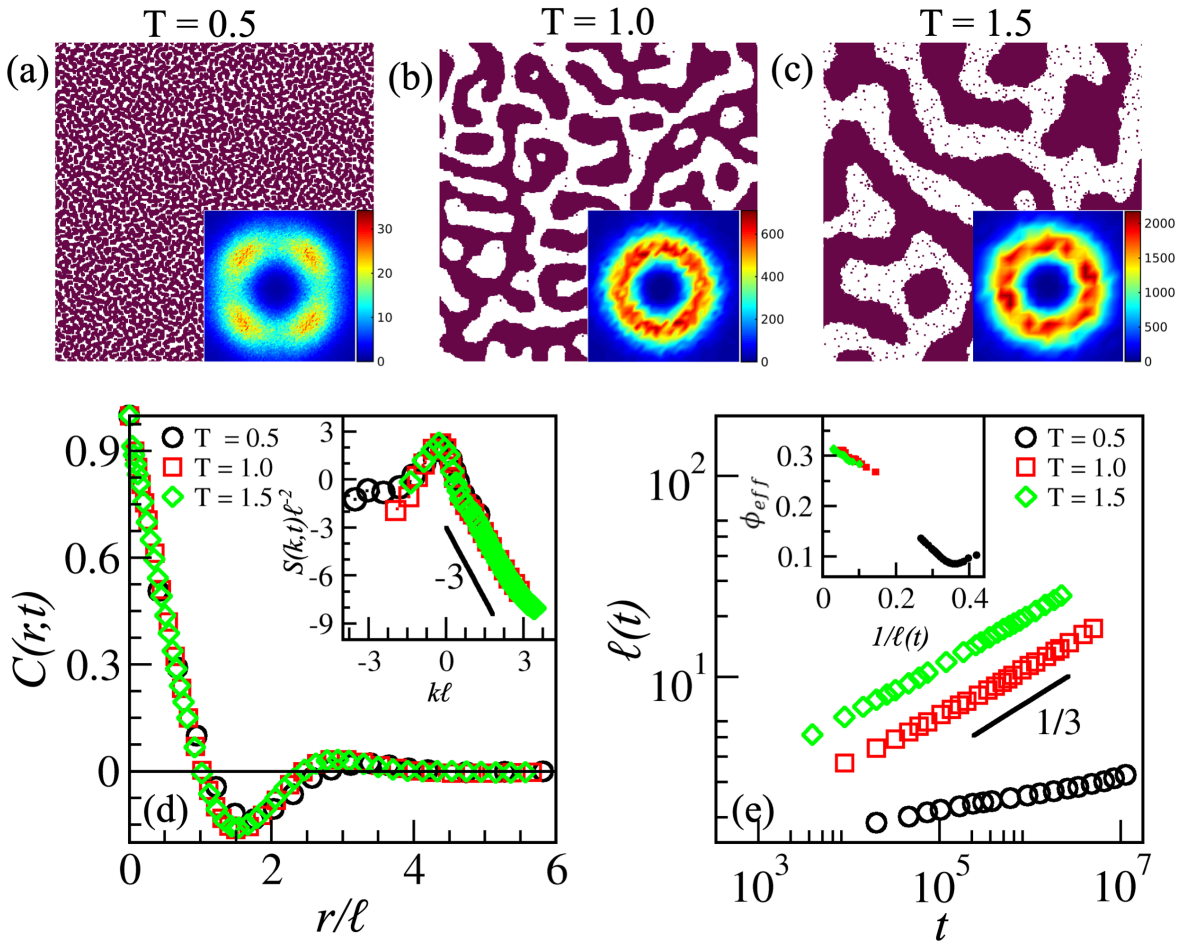

Fig. 5.2: Evolution snapshots for a critical binary (AB) mixture at time $t = 4 \times 10^6$ MCS for temperatures (a) $T = 0.5$, (b) $T = 1.0$, and (c) $T = 1.5$, where the parameter $f_d = 0.0$ represents the pure case. The spatial intensity fluctuation of $S(k_x, k_y)$ is shown in the insets in (a-c). The datasets at $T = 0.5, 1.0$, and 1.5 for the scaling plot of $C(r,t)$ vs. $r/l(t)$ align neatly on a single curve. The plotting of $S(k,t)l(t)^{-2}$ vs. $kl(t)$ is displayed in the inset. The structure factor follows Porod's law, $S(k,t) \sim k^{-3}$ for $k \to \infty$, and is followed by the structural factor tail. The log-log plot of the characteristic length scale, $l(t)$ vs. t, is displayed in (e) for the evolution seen in (a-c). The solid black line represents the expected growth exponent for the pure case, which is $\phi_{eff} = 1/3$. The variation of ϕ_{eff} as a function of $1/l(t)$ is shown in the inset figures.

In order to understand the different morphologies formed by a pure A-B mixture at various temperatures, we plotted the spherically averaged scaled correlation function, $C(r,t)$ vs. $r/l(t)$, as shown in Fig. 5.2(d). The red and green curves, representing $T = 1.0$ and 1.5, respectively, collapse onto a single curve. However, for $T = 0.5$ (black curve), there is a slight deviation at larger domain sizes $(r/l(t) \in (1,3))$ as the domain evolution is still in the transient growth

regime. Additionally, in the inset of Fig. 5.2(d), the scaled structural factor, $S(k,t)l(t)^{-2}$, is plotted with $kl(t)$. It is worth noting that the logarithm of data values has been taken into account on both axes for this and subsequent $S(k,t)l(t)^{-2}$ vs. $kl(t)$ graphs unless otherwise indicated. For larger k values (smaller domain sizes across all temperatures), the scaled structure factor curves neatly overlap onto a master curve. However, for smaller k values (or larger domain sizes), $S(k,t)l(t)^{-2}$ (shown by the black circles) does not overlap with the red and green curves at $T = 0.5$. This suggests that the Ising system follows dynamical scaling on the time scale of our simulation, with a slight deviation at smaller k values at $T = 0.5$ (deep quench). However, the sizable region (tail) of the structure factor ($k \to \infty$) follows Porod's law: $S(k,t) \sim k^{-3}$, which results from the scattering of sharp domain interfaces [190].

The average domain size ($l(t)$ vs. t) time-dependence in Fig. 5.2(e) shows that the evolution kinetics is faster at $T = 0.5$ (black curve) than at $T = 1.0$ and $T = 1.5$ (red and green curves); the former curves follow the LS growth law: $l(t) \sim t^{1/3}$ [238]. The growth exponent, as seen by the black curve, is $\phi \to 0.16$, which is significantly less than the LS diffusive growth exponent. In order to make this clear, we present the growth exponent ϕ_{eff} vs. $1/l(t)$ at various temperatures in the Fig. 5.2(e) inset. The growth exponent $\phi_{eff} \to 1/3$ at $T = 1.0$ and 1.5. However, the growth exponent ϕ_{eff} is far from the LS growth exponent at $T = 0.5$. This suggests that the domain evolution is slower at $T = 0.5$. Throughout most of the simulation, the domain evolution stays in the transient growth regime.

5.3.2 Binary mixtures with the lower fractions of bond disorder: $f_d = 0.02, 0.05$

In order to observe the effect of BD, we first examine the evolution snapshots in Fig. 5.3(a)-(c) at quenching temperatures of $T = 0.5$, 1.0, and 1.5, respectively, at time $t = 4 \times 10^6$ MCS for $f_d = 0.02$. At deep quenching temperatures (Fig. 5.3(a)), much smaller domains are observed, with the lower f_d seemingly having no impact on the evolution morphology. In contrast to the

pure scenario, which results in a smooth and bi-continuous morphology (Figs. 5.2(b)-(c)), we observe the formation of short and interconnected stripes or fragmented lamellar structures when the system is moderately quenched (Fig. 5.3(b) at $T = 1.0$) or shallow quenched (Fig. 5.3(b) at $T = 1.5$). It is apparent from Figs. 5.3(b) and 5.3(c) that the morphology exhibits a certain orientation. The evolution kinetics due to SD are relatively faster when quenched at $T = 1.5$ (Fig. 5.2(c)). Consequently, the short and interconnected stripes formed due to disorder at an early stage of separation kinetics merge to form longer stripes, resembling fragmented lamellar patterns (see Fig. 5.3(c)).

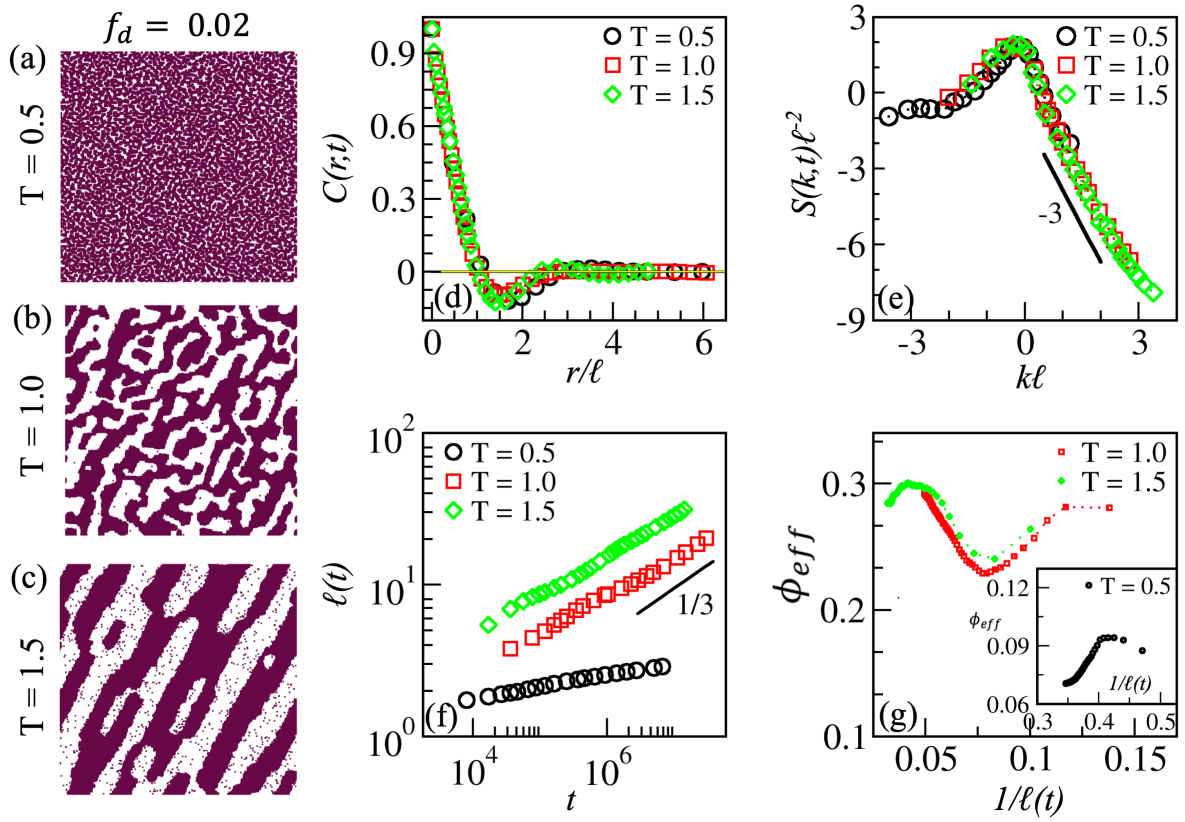

Fig. 5.3: (a-c) Evolution snapshots are shown at $t = 4 \times 10^6$ MCS for $T = 0.5, 1.0$, and 1.5, respectively, for $f_d = 0.02$. Different symbols are used to represent the scaling plots of $C(r,t)$ vs. $r/l(t)$ in (d) and $S(k,t)l(t)^{-2}$ vs. $kl(t)$ in (e) for $f_d = 0.02$ at three quench temperatures. The log-log plot of the length scale $l(t)$ vs. t for all three cases is displayed in (f). The effective growth exponent, ϕ_{eff} vs. $1/l(t)$ is depicted in (g) for $T = 1.0$ and $T = 1.5$, with the inset of (g) showing it for $T = 0.5$.

The direction of the stripe's alignment depends on the fraction of disordered sites for the given system size. The stripes align in the direction of a higher number of disorder sites on the lattice, as displayed in Figs. 5.1(d)-(f). Recall that $J_{ij} = 0$ when any of the two *nn* spins belong to disordered sites. Since phase separation kinetics occurs due to the spin exchange, the most probable locations for this to initiate domain evolution would be in the proximities of disordered sites. Therefore, we start noticing the formation of shorter stripes in the direction of a higher number of disordered sites even at early times, leading to more extended stripe patterns at late times.

We present the scaling functions and effective growth exponents in Figs. 5.3(d)–(g) to demonstrate the effect of lower BD ($f_d = 0.02$) with the quench temperature. When the system is already in the scaling regime, Fig. 5.3(d) displays $C(r,t)$ vs. $r/l(t)$ at three quench temperatures (represented by three distinct symbols) at $t = 4 \times 10^6$ MCS. In Fig. 5.3(e), the equivalent scaled structural factor, $S(k,t)l^{-2}$ vs. kl plot, is shown. The data in Figs. 5.3(d) and 5.3(e) reveals a slight deviation from scaling at larger $r/l(t) \in (1,3)$ after zero-crossing (or smaller $kl(t)$) with the quench temperature. As the quench depths increase, the degree of departure from the scaling for $f_d = 0.02$ is comparable to what we observed for a pure system (Fig. 5.2(d)).

In many cases, the curves show consistent scaling. In Fig. 5.3(f), we can see the characteristic length plotted on a logarithmic scale as $l(t)$ vs. t. The domain size evolves more rapidly for a shallow quench ($T = 1.5$, green curve) compared to a deep quench ($T = 0.5$, black curve), consistent with a pure scenario. For shallow quenches, the system follows the LS growth rule ($\phi \to 1/3$), while the growth exponent for deep quenches is $\phi \to 0.1$, as indicated by the black curve. Fig. 5.3(g) displays the effective growth exponent ϕ_{eff} versus $1/l(t)$ at various temperatures, providing further support for these findings.

The late-time ($t = 4 \times 10^6$ MCS) morphologies for $f_d = 0.05$, quenched at $T = 0.5, 1.0$, and 1.5 are displayed in the evolution snapshots shown in Figs. 5.4(a)-(c). As shown in Fig. 5.4(a),

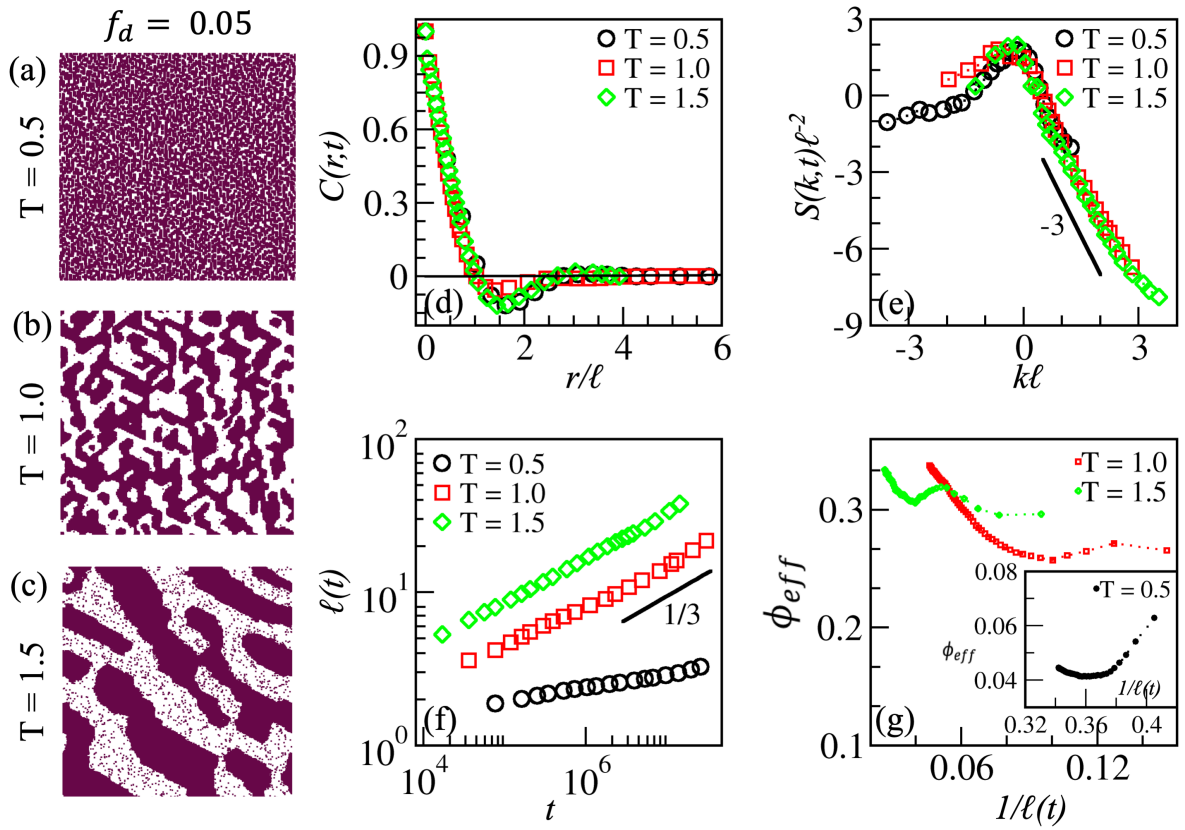

Fig. 5.4: (a-c) Evolution snapshots are shown at $t = 4 \times 10^6$ MCS for $T = 0.5, 1.0$, and 1.5, respectively, for $f_d = 0.05$. Different symbols are used to represent the scaling plots of $C(r,t)$ vs. $r/l(t)$ in (d) and $S(k,t)l(t)^{-2}$ vs. $kl(t)$ in (e) for $f_d = 0.02$ at three quench temperatures. The log-log plot of the length scale $l(t)$ vs. t for all three cases is displayed in (f). The effective growth exponent, ϕ_{eff} vs. $1/l(t)$ is depicted in (g) for $T = 1.0$ and $T = 1.5$, with the inset of (g) showing it for $T = 0.5$.

the influence of BD at deep quench is insignificant, similar to the situation with $f_d = 0.02$. On the other hand, at a shallow quench temperature, we see the formation of longer stripes that resemble the fragmented lamellar (Fig. 5.4(c)), and at a moderate quench temperature, we see the formation of short, connected stripes (Fig. 5.4(b)). Once more, as seen in Fig. 5.1(e) for $f_d = 0.05$, the morphological orientation in both cases is along the higher number of disordered sites. The scaling functions show a more noticeable deviation from the master curve, as seen in Figs. 5.4(d) and 5.4(e) for different quenches denoted by different symbol types, compared to $f_d = 0.02$ (in Fig. 5.3). The tail of the structure factor exhibits a power-law decay:

$S(k,t) \sim k^{-3}$ (Porod's tail) due to scattering from sharp interfaces. The average domain size follows the usual LS power-law growth: $l(t) \sim t^{1/3}$ for higher temperatures, as shown in Figs. 5.4(f) and 5.4(g) with red (at $T = 1.0$) and green (at $T = 1.5$) symbols, respectively. However, the growth at $T = 0.5$ is still the slowest and remains in the transient regime with a growth exponent: $\phi_{eff} \to 0.05$ (inset in Fig. 5.4(g)).

At $T = 0.5$, the growth exponent, ϕ_{eff}, decreases as f_d increases from 0.0 to 0.05 (insets in Figs. 5.2(e), 5.3(g), and 5.4(g)). The reason could be that the small domain structures evolved at deep quench temperature. Instead of transitioning out of the transient growth regime, increasing f_d (from 0.0 to 0.05) causes the morphologies to melt because the system's thermal energy (k_BT) is low at $T = 0.5$, resulting in a reduced effective growth exponent. However, for moderate to shallow quenches with f_d increasing from 0.02 to 0.05, the domain growth swiftly crosses into the diffusive growth phase ($\phi_{eff} \to 1/3$). Figs. 5.2(e), 5.3(f), and 5.4(f) respectively show green curves that indicate a greater prominence of the average domain size at shallow quench temperature. It has been observed that at later stages, ϕ_{eff} surpasses the diffusive growth exponent $(1/3)$ and attains a more significant value for $f_d = 0.05$. One possible explanation for this is that a larger percentage of BD progressively alters the domain interfaces. Consequently, at the domain boundaries where the average spin displacement is proportional to $t^{1/2}$ [15], the random motion (diffusion dynamics) of Ising spins begins alongside the phase separation dynamics. This leads to an increase in the ϕ_{eff} value at a later stage.

At time $t = 4 \times 10^6$ MCS, the morphologies at a shallow quench temperature show long stripes or fragmented lamellae, as seen in Figs. 5.3(c) and 5.4(c). However, the scaling behavior of the system was effectively demonstrated by the spherically averaged structural factor, $S(k,t)$, shown in Figs. 5.3(e) and 5.4(e), rather than by the induced anisotropy caused by the stripe morphology. Thus, in Figs. 5.5(a) and 5.5(b) for $f_d = 0.02$ and $f_d = 0.05$, respectively, we plotted $S(k_x,k_y)$ vs. k_x along the lattice diagonals to emphasize this. The black and red curves

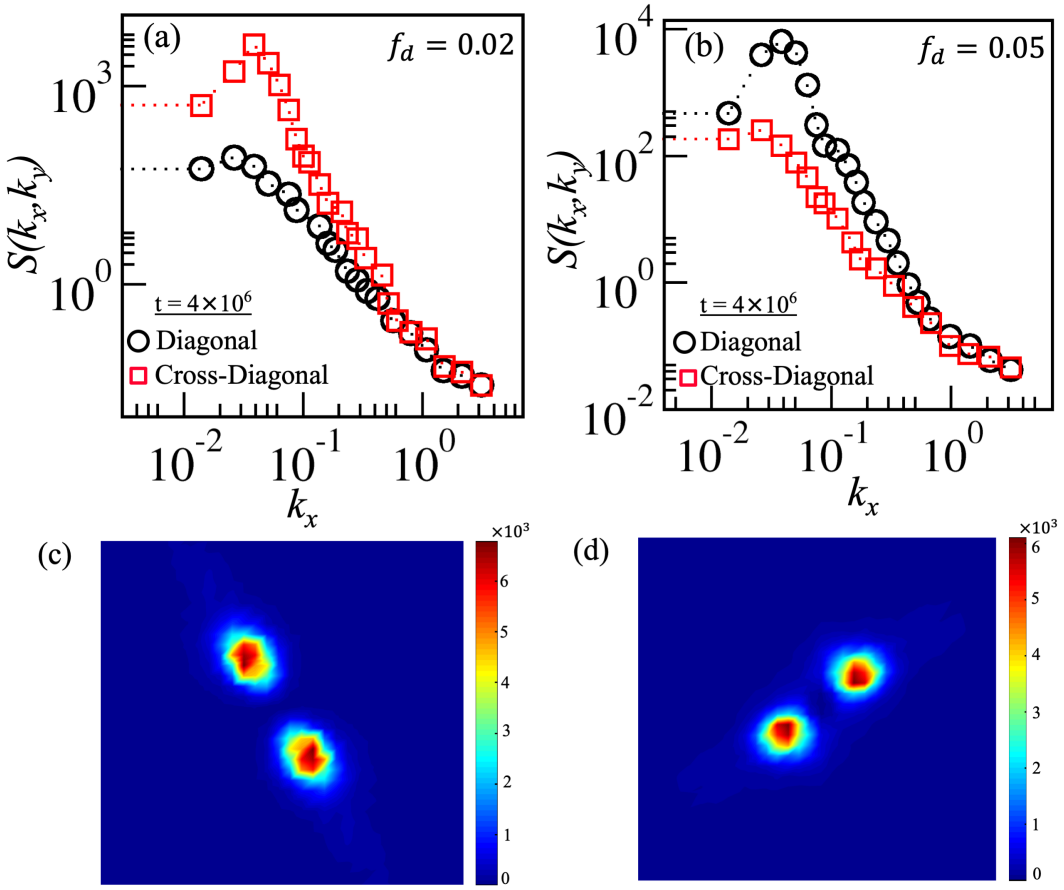

Fig. 5.5: Plots of $S(k_x,k_y)$ at $t = 4\times10^6$ MCS for the following cases: (a) $f_d = 0.02$, and (b) $f_d = 0.05$, at $T = 1.5$. The spatial intensity variation associated with the structure factor, $S(k_x,k_y)$, is displayed in (c–d), revealing the system's orientation and anisotropy.

represent the diagonal and cross-diagonal structural factors. The data is an average of fifty ensembles. The lack of overlap between the $S(k_x,k_y)$ vs. k_x data indicates the existence of structural anisotropy in the system. It is noteworthy that the interchange of black and red $S(k_x,k_y)$ curves for $f_d = 0.02$ in Fig. 5.5(a) and $f_d = 0.05$ in Fig. 5.5(b) demonstrates the change in the alignment of the stripes. The corresponding plots of spatial variation of scattering intensity in Figs. 5.5(c) and 5.5(d) further confirm the change in the orientation of the stripes.

Furthermore, we note that, when $f_d = 0.02$ and $f_d = 0.05$, the green and blue curves in Figs. 5.6(a) and 5.6(b) respectively show similar behavior for $S(k_x,k_y)$ vs.k_x at a moderate quench ($T = 1.0$). However, at a deep quench ($T = 0.5$), the plots of $S(k_x,k_y)$ vs. k_x demonstrate good

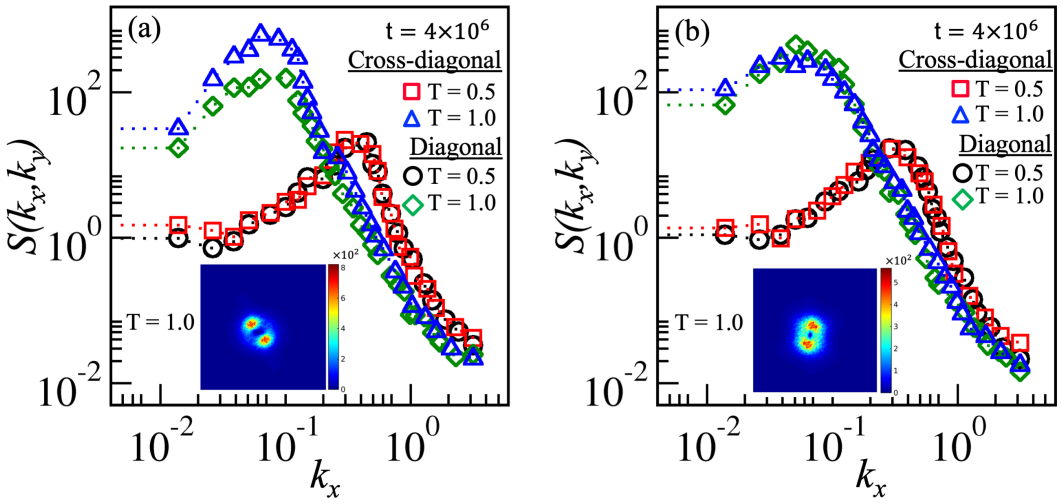

Fig. 5.6: Plot $S(k_x, k_y)$ vs. k_x along the lattice diagonals for $f_d = 0.02$ at $T = 0.5$ (black and red curves) and $T = 1.0$ (green and blue curves) at $t = 4 \times 10^6$ MCS. For $f_d = 0.05$, (b) shows the same data as in (a). The changes in the spatial scattering intensity at $T = 1.0$ for $f_d = 0.02$ and 0.05 are displayed in the insets (a) and (b).

data overlap for the lower fractions of BD, indicated by the black and red symbols in Fig. 5.6, maintaining the system's isotropy. Generally, the evolving morphologies and scaling functions at deep quenching are not significantly affected by the lower f_d values. In contrast, shallow quenching at the same percentages of BD significantly impacts the phase-separating system's length scale, scaling functions, and morphologies. The comparison of anisotropy at lower f_d for $T = 1.0$ and 1.5 is demonstrated in Fig. 5.7.

5.3.3 Binary mixture with a higher fraction of bond disorder: $f_d = 0.1$

In Fig. 5.8(a) at $T = 0.5$, Fig. 5.8(b) at $T = 1.0$, and Fig. 5.8(c) at $T = 1.5$, the evolution morphologies for $t = 4 \times 10^6$ MCS are shown when $f_d = 0.1$. At $T = 0.5$ and for $f_d = 0.02$ and $f_d = 0.05$, there is a slow domain evolution where the system's isotropy is preserved. At $T = 0.5$ with a higher degree of disorder $f_d = 0.1$, the evolving domains start to produce stripes earlier. These stripes eventually evolve into fragmented lamellar patterns, which then transition into perfect lamellar patterns at a later time, $t = 4 \times 10^6$ MCS. This indicates that a larger fraction of BD is sufficient to move the domain evolution out of the slower transient phase

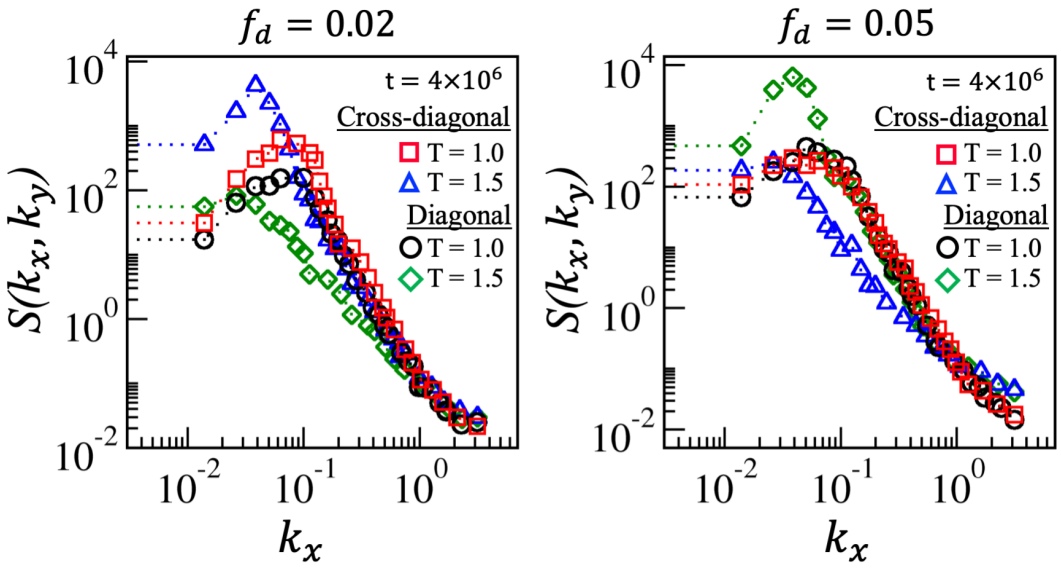

Fig. 5.7: We compare the structure factors without spherical averaging, $S(k_x, k_y)$ vs. k_x along the lattice diagonals at $T = 1.5$ and $T = 1.0$ for $f_d = 0.02$ and $f_d = 0.05$, respectively. The nonoverlapping of curves confirms the presence of structural anisotropy in the system.

when the system is deep-quenched. Consequently, domains start to exhibit the characteristics of stripes. Additionally, a few small random domains of A-type (marked in maroon) are visible within the B-type phases (unmarked) displayed in Figs. 5.8(a)-(c). The system's fuzziness is caused by significant thermal fluctuation (noise) at $f_d = 0.1$. Even at later times, we only observe fragmented lamellar structures with shallow quenches at lower f_d values. Conversely, similar morphologies appear much earlier when $f_d = 0.1$, and eventually, these form into perfect lamellar patterns. As a result, for all quench depths considered here, fully anisotropic structures emerge at later stages when a high fraction of BD is introduced into the system. The evolved stripe patterns are nearly identical for varying system sizes; the orientation of the stripe may change, but the patterns remain consistent. It's important to note that our findings are not influenced by the system size, as illustrated in Figs. 5.9 and 5.10.

In Figs. 5.8(d)-(g), we analyzed the length scales and scaling functions for $f_d = 0.1$ at the asymptotic time limit, $t = 4 \times 10^6$ MCS, for three different quenches, $T = 0.5, 1.0$, and 1.5. As depicted in Fig. 5.8(d) and 5.8(e), the data sets for $C(r,t)$ vs. $r/l(t)$ and $S(k,t)l(t)^{-2}$ vs. $kl(t)$

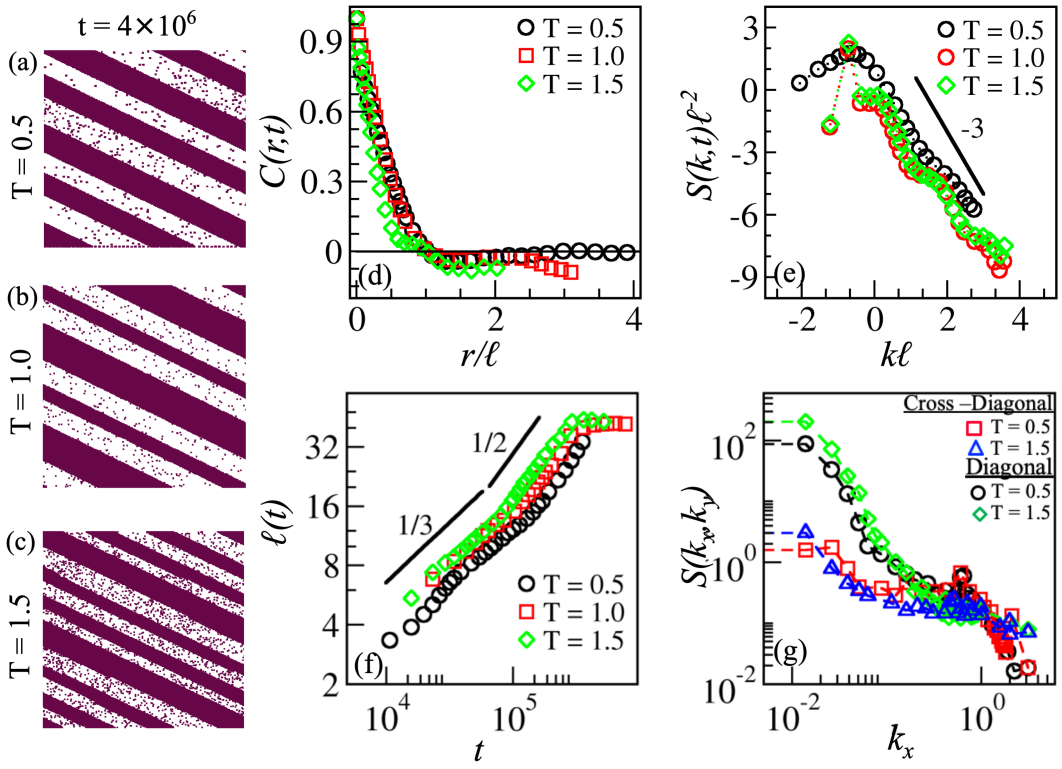

Fig. 5.8: (a-c) Evolution snapshots at $f_d = 0.1$ in the asymptotic limit for $T = 0.5, 1.0$, and 1.5, respectively. (d) Plotting $C(r,t)$ vs. $r/l(t)$ for the evolutions in (a-c) at $T = 0.5$ (black symbol), $T = 1.0$ (red symbol), and $T = 1.5$ (green symbol). (e) Plotting $S(k,t)l(t)^{-2}$ vs. $kl(t)$ for the data sets in (d). (f) A length scale log-log plot with $l(t)$ vs. t. (g) A comparison of $S(k_x,k_y)$ for morphologies at $T = 1.5$ and $T = 0.5$ along the lattice diagonals.

indicate that the black $(T = 0.5)$, red $(T = 1.0)$, and green $(T = 1.5)$ symbols do not overlap. The scaling deviation ensures that the evolved morphologies are not in the same universality class. The solid black line in Fig. 5.8(e) represents the structure factor tail divergence from Porod's rule for $k \to \infty$ with a slope of -3. Porod's law results from the scattering off sharp domain interfaces of small domain structures. The sharp domain interfaces become fuzzier at higher BD due to thermal noise. This causes the well-known Porod's law to be violated. The oscillations in the $S(k,t)l(t)^{-2}$ vs. $kl(t)$ curves confirm that the system is periodic due to its lamellar morphology. The main peak of the structure factor becomes narrower for lower k and more oscillatory for higher k as the quench temperature increases. This suggests that the system gained periodicity due to lamellar patterns at a later time.

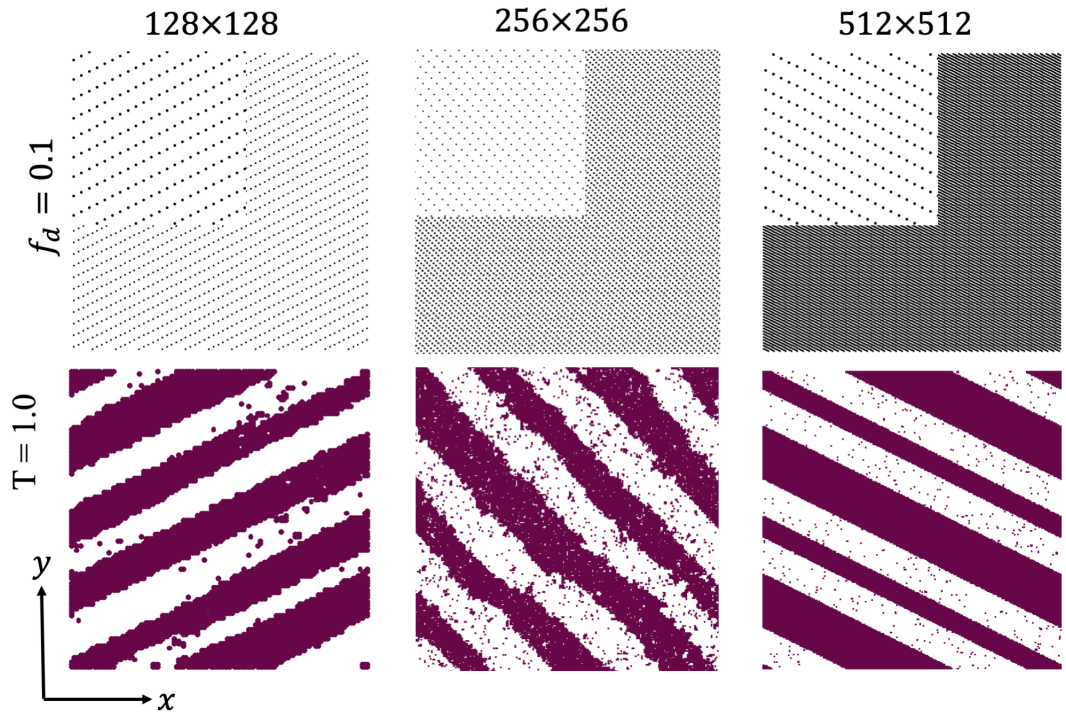

Fig. 5.9: Phase separation for three different system sizes, $N = L^2$ where $L = 128$, 256,and 512, respectively, for a given fraction of disorder, $f_d = 0.1$ at a quenching temperature $T = 1.0$. The top row displays the arrangement of disorder sites, and their top-left corners show the zoomed version of a section of the disorder sites. The bottom row demonstrates the corresponding statistically similar phase-separated morphologies (long stripes or lamellar patterns), oriented in different directions (along with the higher number of disorder sites)

For all quench temperatures shown in Fig. 5.8(f), the characteristic length scale at early times follows the LS growth law ($\phi \sim 1/3$). As the random mobility of spins at domain interfaces increases due to increasing f_d, the growth law gradually transitions to diffusion kinetics ($\phi \sim 1/2$) during the intermediate time. Domain growth freezes at moderate and shallow quenches beyond $t > 10^6$ MCS (noting the red and green curves at $T = 1.0$ and 1.5, respectively). Since the growth kinetics are faster at higher temperatures, the system achieves its equilibrium lamellar morphology earlier for a higher temeperature quench. To compare the anisotropy in the system caused by lamellar morphology produced at deep and shallow quenches, we plot $S(k_x, k_y)$ vs. k_x along the diagonals in Fig. 5.8(g). The black and red curves represent $T = 0.5$, while the green and blue curves are for $T = 1.5$. They show $S(k_x, k_y)$ vs. k_x

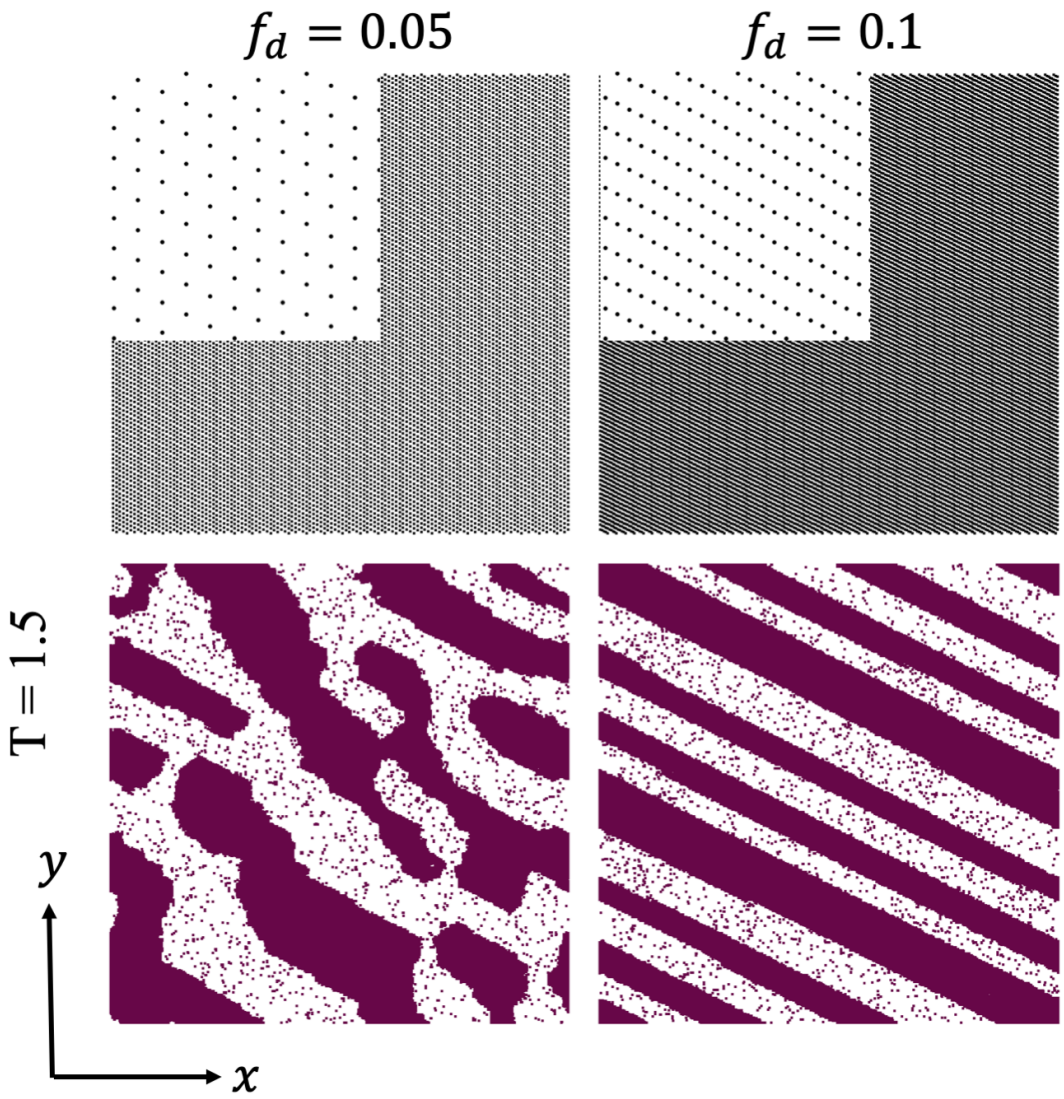

Fig. 5.10: Phase separation for the different fractions of disorder at a fixed system size ($N = L^2; L = 512$), quenched at $T = 1.5$. In the top row, we show the distribution of disorder sites $f_d = 0.05$ and 0.1. The bottom row demonstrates corresponding stripe patterns of different types and orientations (along with the higher number of disorder sites

along the lattice's diagonal and cross-diagonal. When computed along the diagonal (normal to the stripes) rather than cross-diagonally (along the strips), the peak of the structural factor maintains a significantly larger amplitude. The lack of overlap between the $S(k_x, k_y)$ vs. k_x curves indicates the presence of anisotropy within the system. However, a relatively higher peak

strength of $S(k_x, k_y)$ at $T = 1.5$ further suggests that evolved morphologies are more anisotropic at a shallow quench than the morphologies at $T = 0.5$.

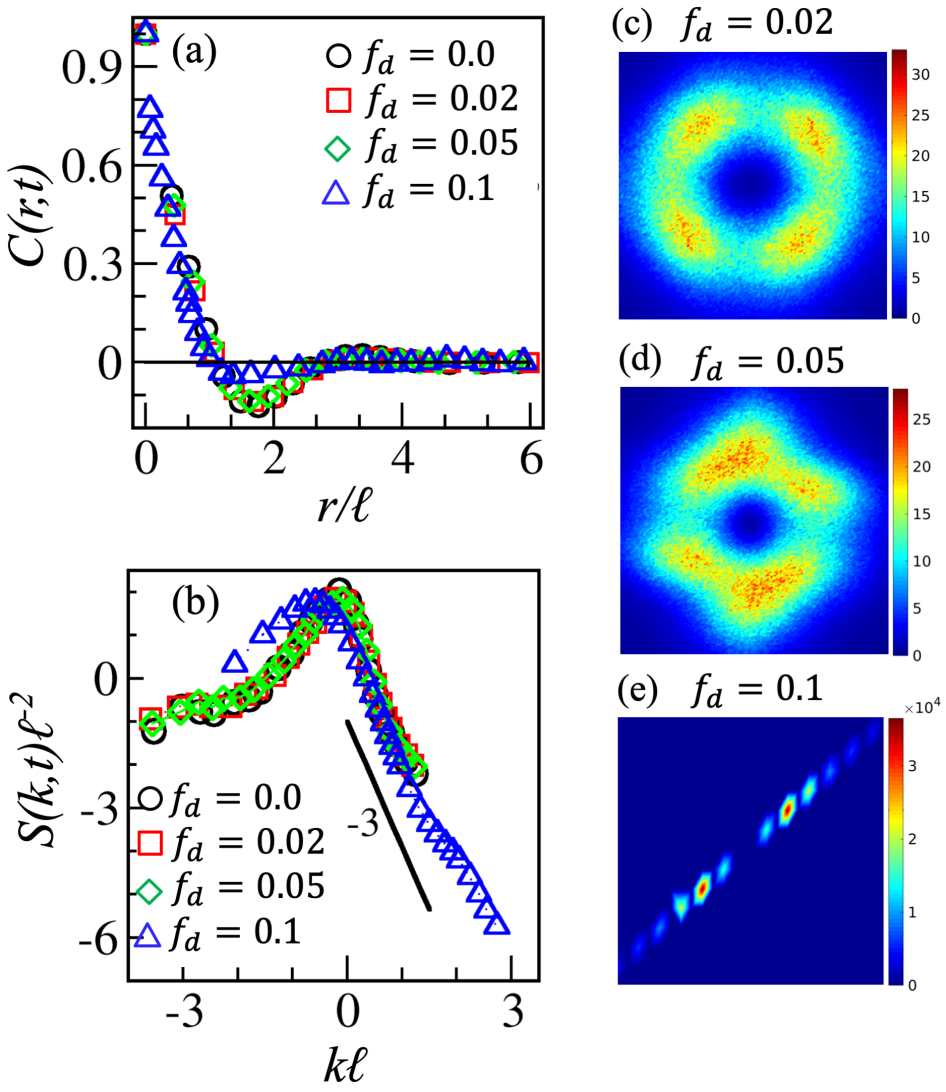

Fig. 5.11: (a) Plot of $C(r,t)$ vs. $r/l(t)$ for different levels of disorder, where $T = 0.5$ for $t = 4 \times 10^6$ MCS and $f_d = 0.0$ (black curve), 0.02 (red curve), 0.05 (green curve), and 0.1 (blue curve). (b) For the datasets in (a), a plot of $S(k,t)l(t)^{-2}$ vs. $kl(t)$ is shown. The variation in scattering intensity over space at $T = 0.5$ is depicted for $f_d = 0.02$ in (c), $f_d = 0.05$ in (d), and $f_d = 0.1$ in (e).

Our observations in Figs. 5.11(a) and 5.11(b) for the later time $t = 4 \times 10^6$ MCS suggest that the scaling functions (the structure factor and the spherically averaged correlation function) for the lower fractions of BD at $T = 0.5$ neatly align with the scaling function of the pure system

($f_d = 0.0$), represented by the black, red, and green symbols. This indicates that the quenched system at $T = 0.5$ and $f_d = 0.0, 0.02$, and 0.05 belong to the same dynamical universality class. In other words, the morphologies appear almost identical to the pure system when evolved at $T = 0.5$ with a smaller f_d. The symmetry in the scattering intensity variation for $f_d = 0.02$ (in Fig. 5.11(c)) and $f_d = 0.05$ (in Fig. 5.11(d)) further justifies the isotropy of the evolved A and B phases, within a minor deviation from the pure case (in Fig. 5.2(a)). Therefore, they belong to the same dynamical universality class. However, when $f_d = 0.1$, the morphology of phases A and B transformed into lamellar patterns. The deviation from the dynamical scaling function (indicated by the blue symbols in Figs. 5.11(a)-(b)) suggests that the system does not belong to the same universality class. This change in symmetry patterns in the scattering intensity variation in Fig. 5.11(e) also confirms this. It is important to note that when the system was quenched at $T = 1.0$ or 1.5, anisotropy was induced even at lower fractions of BD in the form of short/long stripe patterns. However, when BD is increased to $f_d = 0.1$, the strips transform into a broken lamellar pattern, which then becomes a perfect lamellar pattern at later times for all the quench temperatures.

5.4 Summary and conclusion

The study focused on the impact of different percentage of disorder ($f_d = 0.0, 0.02, 0.05$, and 0.1) on the phase separation behavior of a critical binary (AB) mixture. The investigation involved examining the phase separation kinetics at quench temperatures of $T = 0.5, 1.0$, and 1.5 ($T < T_c$). The MC simulation technique was utilized to model the separation kinetics using the conserved (Kawasaki) spin-exchange dynamics on the $2d$ kinetic Ising model. Specifically, the study explored the effects of shallow $(T = 1.5)$ and deep $(T = 0.5)$ quenches at different fraction of disorder f_d on the scaling behavior, characteristic growth laws, and system morphology in the late time limit.

When a homogeneous binary mixture was deeply quenched, a lower f_d had minimal impact on the segregation kinetics. Both the scaled correlation function and the structure factor displayed almost perfect dynamical scaling compared to the pure case. Even at an asymptotic time limit, the domain evolution remained within a transient growth regime. The domain evolution stayed within a transient growth regime even at an asymptotic time limit. The growth exponent, $\phi \sim 0.16$ for the pure case, decreased even further; $\phi \sim 0.05$ for $f_d = 0.05$ due to some randomness at domain interfaces caused by the disorder. Therefore, the growth exponent for a binary mixture at $T = 0.5$(deep quenched) with $f_d = 0.02$ and 0.05 was significantly smaller than the typical *Lifshitz-Slyozov* (LS) growth exponent of $\phi \sim 1/3$.

On the other hand, when the system was shallow quenched at a temperature of $T = 1.5$, the impact of lower fraction of disorder became evident in the evolution process. To facilitate a better comparison, we also conducted a quench at a moderate temperature of $T = 1.0$. A pure system exhibited typical evolution kinetics at these temperatures. However, for lower fractions of disorder quenched at $T = 1.0$, the system formed short and interconnected stripe patterns, while a longer and fragmented lamellar morphology was observed at $T = 1.5$. These morphologies were influenced by a higher number of disorder sites and led to the formation of anisotropic morphologies. This deviation from dynamic scaling became more pronounced as the fraction of disorder increased at the shallow quench temperature. Nonetheless, the growth law remained consistent with the LS power-law growth with a deviation to a slightly higher growth exponent in the asymptotic time limit.

When there is a high fraction of disorder ($f_d = 0.1$), we observed the formation of long fragmented strips early for all the temperatures we studied. These strip patterns then gradually transformed into a perfect lamellar pattern with different periodicity. As a result, we noticed a significant difference in the dynamic scaling behaviors at various temperatures as time progressed. Initially, the growth of the domains followed the LS growth law: $\phi \sim 1/3$, and then transitioned to diffusion dynamics: $\phi \sim 1/2$ during intermediate time. However, our

simulations showed that the domain growth remained finite once the system reached a stable lamellar morphology. The domain growth at $T = 1.5$ saturating earlier than at $T = 1.0$. We haven not observed saturation in the length scale for $T = 0.5$ yet, but it may occur at a much later time.

The pattern formation in the disordered system is of great technological importance. Our model can be integrated to understand a wide variety of physical phenomena such as the structural evolution in the biological system (e.g., the iridescent color patterns of bird feathers observed due to refraction of incident light from the phase-separated frozen nanostructures), self-organizing spatial patterns in ecological systems (e.g., mussel beds, etc.). Furthermore, the phase separation kinetics in multiphase fluid and mineral exsolution can be easily explained. Finally, our simulation results provide a general framework for the experiments on domain growth in kinetic Ising systems with the bond disorder. In the future, we aim to address its effect and quench depths for the Ising systems in $3d$ where similar experiments have not yet been performed. Thus, we hope our simulation results offer essential guidelines for future studies.